Pergamon

Int. J. Heat Mass Transfer. Vol. 39, No. 12, pp. 2473–2484, 1996

0017-9310/96 $15.00+0.00

0017-9310(95)00323-1

Mixed convection in straight and curved channels with buoyancy orthogonal to the forced flow

P. M. LIGRANI and S. CHOI

Convective Heat Transfer Laboratory, Department of Mechanical Engineering, University of Utah, Salt Lake City, UT 84112, U.S.A.

(*Received* 23 *March* 1995 *and in final form* 23 *August* 1995)

Abstract—Mixed convection in straight and curved channels is investigated when buoyant forces are perpendicular to the bulk flow direction. Grashof numbers are based on temperature difference range from 0 to 50×10^6, and Reynolds numbers are based on channel width range from 343 to 2057 which gives laminar and transitional forced flow. Four difference regimes of behavior are apparent: pure natural convection, mixed convection with strong buoyancy, mixed convection with weak buoyancy and pure forced convection. Differences in behavior between these different regimes are discussed, along with curvature influences, the effects of buoyancy on forced flow behavior, and Nusselt number correlations for the two mixed convection regimes. Copyright © 1996 Elsevier Science Ltd.

INTRODUCTION

In the past 10–15 years, there has been much interest in the effects of buoyancy on laminar internal flows. Arrangements of importance include geometries with buoyant forces both *aligned* and *orthogonal* to the forced flow direction because both situations arise in a wide variety of applications, including electronics cooling, heat exchangers, internal turbine blade cooling systems, ducting systems used in space vehicles, nuclear reactors, chemical reactors, passages in biological systems, and ducting in internal combustion engines. Alterations from buoyancy in all of these situations can be quite significant.

Investigations of *aligned* laminar mixed convection in *vertical* channels are described by a number of investigators [1–6]. Of these, Churchill and Usagi [2], Churchill [3] and Shai and Barnea [5] present mixed convection Nusselt number correlations expressed in terms of pure forced convection and pure natural convection values for both assisting and opposing mixed convection. Chilukuri and Humphrey [4] include the influences of buoyancy in their investigation of laminar forced convection in curved channels with heat transfer. Their steady numerical predictions were made of developing laminar flow in a curved square channel with buoyant forces both aligned with and opposed to the main flow direction. At a Dean number of 367, Nusselt numbers increase by as much as 10% if buoyancy assists bulk flow motion, and decrease by as much as 13% when buoyancy opposes the bulk flow.

There are also numerous studies of mixed convection in *horizontal* channels with buoyant forces *orthogonal* to the forced flow (and directed across the narrowest dimension of the channel cross section). The earliest experimental studies reveal significant heat transfer enhancement compared to forced convection alone from buoyancy induced longitudinal vortices [7–13]. One early numerical investigation considers factors which alter the onset of the longitudinal vortices [14]. Other numerical predictions indicate large entry length changes with different magnitudes of buoyancy, and important differences between fully developed and entry flows [15–21]. Additional clarification of these issues, including the effects of the buoyancy induced longitudinal vortices on transition to turbulence, are provided in later experimental work [22, 23]. Other recent numerical investigations address surface heat transfer in horizontal channels with mixed convection [24–26], or the onset, structure, development and heat transfer augmentation of buoyancy induced instabilities [27–32]. The most recent experimental investigations consider similar topics [31, 33–34].

Like the *horizontal* channel studies just mentioned, the present study also considers mixed convection with buoyant forces orthogonal to the forced flow. The most important differences are: (i) the *vertical* parallel plates of our channel, arranged so that buoyancy is directed across the widest dimension of the channel cross-section and (ii) the amount of curvature. Figure 1 shows the coordinate system and geometry employed. The channel aspect ratio ($2l/d$) is 40, top and bottom boundaries are closed, and constant heat flux boundary conditions are applied. Figure 1 also shows that the channel has curved and straight portions, and that gravity is directed in the positive Z-direction.

Mixed convection in a curved channel deserves

NOMENCLATURE

d	channel height
D_H	hydraulic diameter
g	gravitational acceleration
Gr	Grashof number based on temperature difference, equation (7)
Gr^*	Grashof number based on heat flux, equation (8)
h	spanwise-averaged heat transfer coefficient, equation (1)
k	thermal conductivity
l	length of half channel span
Nu	spanwise-averaged Nusselt number, equation (2)
Pe	molecular Peclet number
Pr	molecular Prandtl number
Re	Reynolds number, Ud/ν
t	time-averaged local temperature
t_m	mixed-mean temperature
t_w	local wall temperature
u_0	streamwise mean velocity
U	bulk mean velocity
V_c	natural convection velocity scale
x	streamwise (bulk forced flow direction) distance from location where heating begins
X	streamwise (bulk forced flow direction) distance from channel inlet at nozzle exit
Y	distance normal to channel surfaces from the concave surface
Z	spanwise distance from channel spanwise centerline.

Greek symbols

α	$(\beta\Delta t)/(\beta\Delta t)_{NC}$, as in equation (12)
β	volumetric coefficient of thermal expansion
ν	kinematic viscosity
Δt	local $(t_w - t_m)$.

Subscripts

NC	natural convection
FC	forced convection.

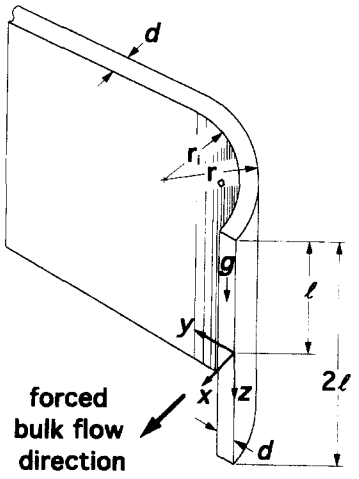

Fig. 1. Channel coordinate system and geometry.

study because: (i) of its technological importance and (ii) it is capable of producing a particularly interesting and complex flow field wherein centrifugally induced secondary flows interact with secondary flows induced by buoyancy. However, in spite of these considerations, there are no other experiments known on such an arrangement other than the present study. The only other study to consider a flow with buoyant influences in curved channels is numerical [4], and even recent experimental studies of orthogonal mixed convection in straight channels [22, 23, 31, 33, 34] are rare.

The present experiment was thus motivated by fundamental interest in mixed convection in a geometry not previously studied, and by an effort to understand the influences of buoyancy on flows in curved and straight passages. The data are also intended to aid the development of codes for the prediction of complex elliptic flows. Included are descriptions of the differences in behavior between natural, mixed and forced convection regimes, and the changes to local Nusselt numbers which result as the magnitudes of buoyant motions are altered relative to straight and curved forced convection.

CURVED CHANNEL AND OTHER EXPERIMENTAL APPARATUS

A schematic of the rectangular cross-section channel is shown in Fig. 2. The interior rectangular cross-section is 1.27 cm × 50.1 cm, giving the aspect ratio of 40 mentioned. This large aspect ratio is chosen to minimize the influences of side walls and the Eckmann vortices which form there, and to provide adequate space for repeated spanwise periodicity across the channel span. The channel allows longitudinal and spanwise thermal expansion of channel surfaces as they are heated through non-rigid securing of channel walls on skids and the use of air seals along the lengths of the walls near spanwise edges. Skogerboe [35], Schallert [36] and Choi [37] provide additional details of the design and construction of the channel.

Prior to entering the channel, a number of devices are used to reduce spatial non-uniformities in the flow, including a circular lip inlet, an aluminum honeycomb, and three wire screens. These are followed by

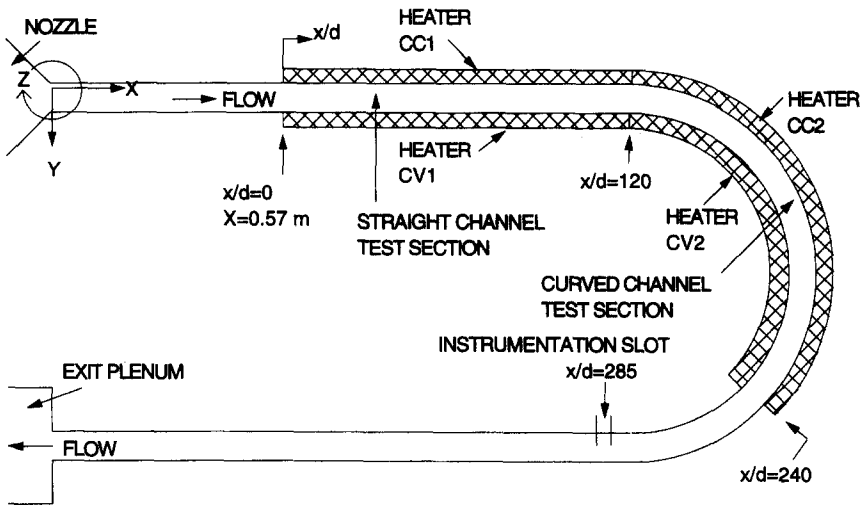

Fig. 2. Schematic of the channel.

a 20 : 1 contraction ratio nozzle, designed using a fifth-order polynomial with respect to streamwise distance to ensure that the flow remains laminar, un-separated, and without any Görtler vortices as it enters the channel. After exiting the inlet nozzle, air first enters a straight section, 2.44 m in length, of which the last 1.52 m is heated, with interior dimensions of 1.27 cm × 50.8 cm. The straight section provides hydrodynamically fully developed flow for Reynolds numbers less than 3800. The fluid then enters a 180° curved channel section with a convex surface radius of 59.69 cm and a concave surface radius of 60.96 cm. The interior walls of the heated section are made of 0.08-cm thick Lexan.

Upon exiting the curved section, the air then enters a second straight section also with a length of 2.44 m. A 5.08-cm wide slot is present on this section attached to the convex wall which allows insertion of a probe into the channel to measure outlet mixed mean temperatures. Figure 2 shows the location. Two thin foam strips line the slot to provide an air tight seal between the channel interior and exterior as the probe is traversed. As flow leaves the second straight portion, it passes through four screens, a honeycomb, a diffuser with a total angle of 3°, and finally into the first of two plenum chambers maintained at vacuum pressure. The blower used to depressurize the plenum chambers is an ILG Industries 10P type, capable of producing 10.2 cm of water vacuum at 4.82 $m^3\ min^{-1}$ volumetric flow rate. Channel air mass flow are determined from measurements of the pressure drop across an orifice plate with a 3.81 cm hole located in piping between the two plenums.

Four etched foil heaters, manufactured by the Electrofilm Corporation, are installed to heat both the concave and convex surfaces of the channel, all at the same power dissipation rates, to produce uniform heat flux boundary conditions at the channel walls. The dimensions of each heater are 38.1 cm × 152.4 cm. As shown in Fig. 2, CC1 and CV1 designate the two heaters on the concave and convex surface of the straight section, respectively, and CC2 and CV2 designate the heaters on the concave and convex surfaces of the curved section, respectively. To minimize heat conduction away from the test surfaces, the outsides of the channel from just upstream of the heaters CC1 and CV1 to the slot located downstream of heaters CC2 and CV2 is insulated with 5–7 cm of black foam insulation manufactured by the Halstead Company.

One hundred copper–constantan thermocouples are placed just beneath Lexan channel surfaces (on sides not exposed to the air stream) to allow spatially resolved surface temperature measurements to be made. Twenty-five thermocouples are placed beneath each of the CC1, CV1, CC2 and CV2 heater surfaces in five spanwise rows of five per row so that spanwise-average Nusselt numbers can be measured at different streamwise locations. The first row of thermocouples is located 103.64 cm from inlet or 15.24 cm from the leading edge of the first heater. Each additional row is spaced 30.48 cm apart in the streamwise direction. The thermocouples are placed over a spanwise distance of approximately 10.16 cm on each side of the centerline. Forty additional copper–constantan thermocouples are placed between layers of insulation to determine conduction heat losses. Two additional thermocouples are used to measure mixed mean temperature at the channel inlet and mixed mean temperature at the channel outlet.

Voltages from the 142 thermocouples used to deduce temperatures are read sequentially by Hewlett-Packard type T20 relay multiplexer card assemblies for T type thermocouples. These assemblies are installed in a HP3497A low-speed Data Acquisition/Control Unit and a HP3498A Extender. This system provides thermocouple compensation electronically such that voltages for type T thermocouples are given relative to 0°C. The control unit and extender are connected to a Hewlett-Packard 9836A computer which processes voltages from the 142 ther-

mocouples which are then recorded into data files along with corresponding temperatures.

EXPERIMENTAL PROCEDURES

Nusselt numbers

As the test conditions are set-up, heater power levels are adjusted to provide a constant surface heat flux boundary condition along the instrumented test surfaces. The channel is heated to thermal equilibrium, during which channel surfaces expand to the sizes they assume as measurements are made. After reaching thermal equilibrium, measurements are made to determine local Nusselt numbers.

Local heat transfer coefficient and local Nusselt number are given by:

$$h = \dot{q}''_{\text{conv}}/(t_w - t_m) \tag{1}$$

and

$$Nu = hD_H/k \tag{2}$$

respectively. Convective heat flux $\dot{q}''_{\text{conv}}$ in equation (1) is determined using an equation of the form:

$$\dot{q}''_{\text{conv}} = (IV - \dot{q}_{\text{cond}})/A \tag{3}$$

where A is the surface area of one segment of the heated test section and $\dot{q}_{\text{cond}}$ is the conduction power loss for the segment. Each segment is 38.1 cm × 30.48 cm with a row of five thermocouples along the center, and comprises 10% of the heated test section on each channel surface (or 20% of the area of each heater CV1, CC1, CV2 or CC2). To determine the power supplied to each heater segment, the power supplied to each heater is first determined from measurements of current and voltage drop. The product of this current and voltage drop is then divided by five to obtain IV.

Energy balances are used to determine t_m, the local mixed mean temperature at any streamwise channel location in equation (1). The form of the energy balance equation used for this purpose is given by:

$$t_m = t_{\text{m-inlet}} + (\dot{q}''_{\text{conv}} b\,\Delta x)/\dot{m}C_p \tag{4}$$

where $t_{\text{m-inlet}}$ is the mixed mean temperature at the channel inlet, b is the spanwise width of the heated surface, Δx is the streamwise distance from the beginning of heating to the streamwise station of interest, $\dot{m}$ is the air mass flow rate and C_p is air specific heat.

As mentioned earlier, calibrated copper–constantan thermocouples are used to determine local wall temperatures at 100 locations along the channel surfaces. Because t_w in equation (1) represents the temperature of the surface just adjacent to the air stream, temperatures measured by the thermocouples must be corrected since a 0.08 cm thick Lexan sheet separates them from the air stream. The correction for each thermocouple then accounts for the temperature drop resulting from the contact resistance between the thermocouple and the Lexan, as well as for conduction through the Lexan. The equation which accounts for these corrections to give corrected wall temperature t_w is given by

$$t_w = t_{\text{w-uc}} - C_R \dot{q}''_{\text{conv}} \tag{5}$$

where $C_R = 0.0034^\circ\text{C m}^{-2}\text{ W}^{-1}$ determined from experiment and $t_{\text{w-uc}}$ is the uncorrected temperature measured by each thermocouple.

Nusselt numbers measured locally at five different spanwise locations (Z/d equals -8, -4, 0, 4 and 8) provide checks on measurement procedures at 10 different x/d from 12 to 228 [36]. At high Reynolds numbers (>2000), excellent spanwise uniformity within 0.3 Nusselt number units indicates minimal spanwise conduction losses. At lower Reynolds numbers less than 300–400, small spanwise variations with Z/d result from natural convection influences.

The experimental uncertainty of Nusselt numbers based on a 95% confidence level is ±4%.

Exit mixed mean temperature

To calculate the local mixed mean temperature at the exit of the heated test section, a thermocouple and a miniature five hole pressure probe [38, 39] are separately inserted through the convex wall slot. Each is then traversed over a spanwise/normal plane using an automated two-dimensional traversing device controlled by the 9836A computer. From the measurements made during these surveys, the mixed mean temperature is given by:

$$t_m = \frac{1}{A_{ch}U}\int_{A_{ch}} u_0 t\,\mathrm{d}A \tag{6}$$

where A_{ch} is the cross-sectional area of the channel. The mixed-mean temperature from this direct measurement approach and from energy balances [equation (4)] are compared at $x/d = 285$. Values for different Re are given in Table 1. The agreement for the entire range of Reynolds numbers studied verifies the procedures employed to determine spanwise-averaged Nusselt numbers including conduction energy balances and energy balances to calculate mixed-mean temperatures. Additional details are provided by Choi [37].

MIXED CONVECTION WITH WEAK BUOYANCY

Nusselt number dependence on Grashof number

Figure 3 illustrates typical mixed convection Nusselt number behavior when buoyancy is relatively

Table 1. Mixed mean temperatures at $x/d = 285$

Re	t_m [°C] Energy balance equation (4)	t_m [°C] Direct measurement equation (6)	t_m [°C] Channel inlet
1028	40.8	42.4	23.3
1371	39.5	40.7	22.5
1713	39.4	40.1	24.1

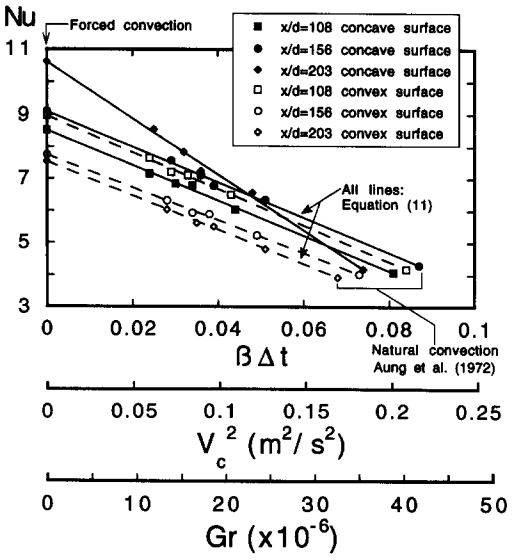

Fig. 3. Measured mixed-convection Nusselt numbers, deduced forced convection Nusselt numbers, and natural convection Nusselt numbers as dependent upon Gr, V_c^2, and $\beta\Delta t$ to illustrate mixed convection with weak buoyancy for $Re = 1371$.

weak. Here, measured Nu are plotted as a function of Gr, V_c^2 and $\beta\Delta t$ for a Reynolds number of 1371. Of these different abscissa scales, Nu data points are plotted at exact corresponding values of $\beta\Delta t$ and V_c^2. The Gr scale in Fig. 3 is then only approximate because of variations of kinematic viscosity with temperature. $\beta\Delta t$ was chosen for the abscissa because it is directly related to the magnitude of natural convection through its proportionality to Grashof number, given by

$$Gr = gl^3\beta\Delta t/\nu^2. \tag{7}$$

The Grashof number can also be written in terms of convective heat flux using

$$Gr^* = gl^3 d\beta\dot{q}''_{\text{conv}}/k\nu^2 \tag{8}$$

which is equivalent to $Gr^* = GrNu/2$. A characteristic velocity scale, induced by natural convection, is then given by

$$V_c = (Gr)^{1/2}\nu/l \tag{9}$$

or alternatively

$$V_c = (gl\beta\Delta t)^{1/2}. \tag{10}$$

Different sets of $\beta\Delta t$, V_c and Gr for a particular Reynolds number, flow condition, channel surface, and streamwise station are thus produced using different power levels within the test surface heaters. These in turn give different Nusselt numbers, as shown in Fig. 3. The mixed convection Nu in Fig. 3 result from contributions due to buoyancy-induced motions and forced motions with magnitudes which then vary with the ratio of natural convection influence to forced convection influence. Of these two effects, the one associated with buoyancy varies significantly with Gr (and $\beta\Delta t$), whereas forced motions contributing to Nu are independent of Gr (and $\beta\Delta t$).

Pure natural convection Nusselt numbers

Nusselt numbers for pure natural convection are also included in Fig. 3, determined from results presented by Aung *et al.* [40] based on experimental conditions corresponding to the largest *measured* mixed convection V_c^2 and $\beta\Delta t$ from the present study. As shown, the values lie in the right-hand portion of the figure, and are plotted at V_c^2 and $\beta\Delta t$ values determined from linear extrapolation from the mixed convection data. Thus, the Aung *et al.* [40] results in Fig. 3 are forced to be a linear extension of our measured mixed convection data. The V_c^2 values range from 0.17 to 0.22 $m^2\ s^{-2}$, and the $\beta\Delta t$ values range from 0.07 to 0.09. Corresponding Aung *et al.* [40] Grashof numbers give the same V_c^2 and $\beta\Delta t$ within ± 0.001 units of $\beta\Delta t$. Careful inspection of these natural convection Nu data reveals a consistent small increase as $\beta\Delta t$ increases from 0.07 to 0.09, and as Gr increases from 32×10^6 to 42×10^6. Corresponding natural convection velocity scales are above 0.4 m/s which are significant, especially near walls, considering the bulk velocity from forced convection is 1.68 m s^{-1} at $Re = 1371$.

Determination of forced convection Nusselt numbers

One of the most striking features of the mixed convection Nusselt number data in Fig. 3 is their linear dependence upon V_c^2 and $\beta\Delta t$. These parameters are used for the abscissa scales for this reason and because the linearity is much better than when Nu data are exactly plotted *vs* Gr. Figure 3 also shows that natural convection Nu [40] are lower than mixed convection values ($Gr = 10\times10^6$–30×10^6, $\beta\Delta t = 0.02$–0.06), and form a natural extension of the lines through each set of mixed convection data points for a particular x/d and channel surface.

Because of this behavior, forced convection Nu can be determined from the mixed convection data by extrapolating lines through the data to $Gr = 0$ and $\beta\Delta t = 0$. $Gr = 0$ and $\beta\Delta t = 0$, of course, represent forced convection where the buoyancy induced velocity scale is zero. *Measured* mixed convection Nu in Fig. 3 are thus located on straight lines between pure forced convection and pure free convection values when buoyancy influences are relatively weak. The ranges of parameters which characterize this type of behavior are discussed later in the paper.

Correlation of data for mixed convection with weak buoyancy

Because of the linear behavior, mixed convection Nusselt numbers such as the ones in Fig. 3 are well correlated using an equation of the form

$$Nu = Nu_{NC}\alpha + Nu_{FC}(1-\alpha) \quad (11)$$

where

$$\alpha = (\beta\Delta t)/(\beta\Delta t)_{NC} = (V_c/V_{c\text{-}NC})^2 \approx Gr/(Gr)_{NC} \quad (12)$$

with α ranging from 0 to 1. Equation (11) is valid with weak buoyancy in curved and straight channels when buoyancy induced flow and pressure gradient induced flow are perpendicular. The assisting mixed convection Nu relations for parallel flow fields from Churchill and Usagi [2], Churchill [3], and Shai and Barnea [5] are also expressed in terms of Nu_{NC} and Nu_{FC} like equation (11).

Equation (11) is also consistent with the application of linear superposition to mixed convection and the linear dependence of $\dot{q}''_{conv}$ on Δt. Prior to the work of Park and Tien [41], linear superposition has generally been widely applied to force convection but only to natural and mixed convection when local buoyancy effects are negligibly small and aligned with the bulk flow. This is because of the coupling effects and the non-linearity of the field equations with natural and mixed convection. Park and Tien [41] overcame this limitation for these flows with a superposition scheme based on similarity solutions to the field equations which give a non-linear dependence of $\dot{q}''_{conv}$ on Δt. This scheme does not seem to fit the present experiment with *weak* buoyancy wherein the perpendicular bulk flow and buoyancy induced fields seem to reduce the non-linearity and coupling in the field equations whenever $Re \geqslant 686$. As a result, the temperature field behaves like a mixed convection environment with negligibly small buoyancy, superposition is linear, and $\dot{q}''_{conv}$ is linearly dependent upon Δt.

Nusselt number variations with x/d

Nusselt number data for all three convection regimes at $Re = 1371$ are shown in Figs. 4 and 5 as a function of x/d. Concave surface Nusselt numbers are given in the first of these figures and convex values are presented in the second. Gr values given in the captions are average values determined over the length of the test section. The straight portion of the channel extends from x/d of 0–120 and the curved position from 120 to 240.

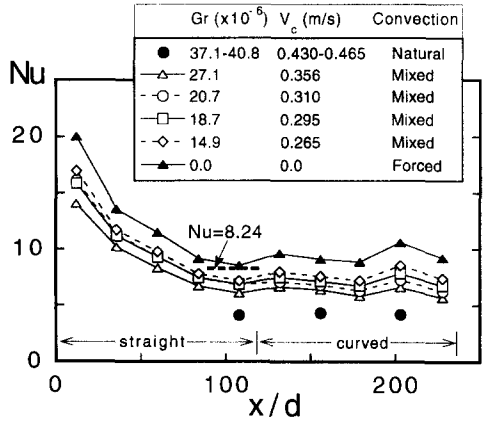

Fig. 4. Measured mixed-convection Nusselt numbers, deduced forced convection Nusselt numbers, and natural convection Nusselt numbers as dependent upon x/d for straight and *concave* surfaces at $Re = 1371$. Natural convection Nusselt numbers are from Aung *et al.* [40].

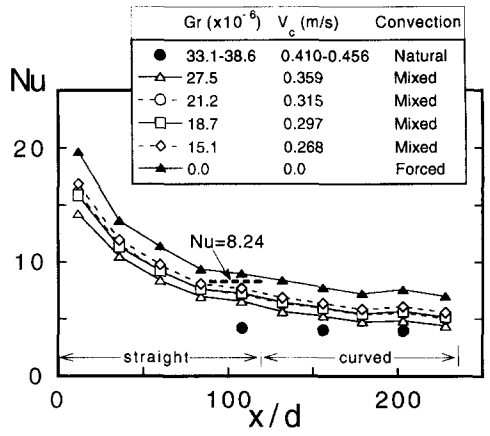

Fig. 5. Measured mixed-convection Nusselt numbers, deduced forced convection Nusselt numbers, and natural convection Nusselt numbers as dependent upon x/d for straight and *convex* surfaces at $Re = 1371$. Natural convection Nusselt numbers are from Aung *et al.* [40].

As for the results in Fig. 3, Nu data in Figs. 4 and 5 show a systematic decrease with increasing Gr and V_c. Chilukuri and Humphrey [4] observe similar trends in a curved channel when buoyancy opposes the forced flow. Because the Nu decreases with Gr in the present study occur at all x/d, the qualitative character of the changes are the same regardless of thermal boundary layer development, and regardless of whether results are obtained in the straight or curved portions of the channel. Pure forced convection data for $Gr = 0$ (extrapolated from the mixed convection data) lie at the top of each distribution in Figs. 4 and 5, and pure natural convection data [40] for $Gr = 33.1\text{-}40.8 \times 10^6$ lie at the bottom. Mixed convection data at Gr from 14.9×10^6 to 27.5×10^6 are then in between the pure forced convection and pure natural convection data.

Checks of pure forced convection Nusselt number behavior

Referring to the forced convection Nu data in the straight portion of the channel at x/d from 0 to 120, comparison of results in Figs. 4 and 5 shows that values from the two heated surfaces match at each streamwise location. This is important because it provides a check on temperature and heat transfer coefficient measurements and shows that energy balances are self-consistent. Additional verification of procedures and techniques is provided by trends of $Gr = 0$ data for $x/d < 120$ which decrease with streamwise distance consistent with thermal entry length behavior. Some deviation from pure forced con-

vection behavior is expected especially for $Re < 700$ ($Pe < 6$), because thermal boundary layers at small x/d are relatively thin and located entirely in low velocity portions of the velocity boundary layer where buoyancy induced velocities and motions dominate. Thus, even though buoyancy may have little influence on the bulk flow as a whole, it may still be influential locally near walls.

Figures 4 and 5 also illustrate spanwise-averaged forced convection Nusselt numbers ($Gr = 0$) which approach the expected value of 8.24 as thermal boundary layers in the straight portion of the channel merge and become fully developed at $x/d = 108$. $Nu = 8.24$ is expected from a simple derivation for fully developed laminar forced convection between two infinite parallel plates with constant heat flux boundary conditions. Similar conclusions are reached regarding the $x/d = 108$, $Gr = 0$ extrapolated data in Fig. 3. Here, results from both concave and convex surfaces approach values near 8.24 as abscissa values decrease to the forced convection limit at $Gr = 0$ (also $\beta\Delta t = 0$ and $V_c^2 = 0$). Small differences from the expected value at $x/d = 108$ may be due to finite span effects, residual buoyancy effects, slight data scatter, and/or slightly different thermal boundary layer development at different Reynolds numbers [42]. However, in spite of any deviations due to these effects, forced convection Nusselt numbers in Figs. 3–5 provide strong evidence of the validity of the experimental approach and results.

Effects of thermal boundary layer development

Regions where Nu decrease with x/d in Figs. 4 and 5 are regions where the channel thermal boundary layers are less than fully developed. At a particular Gr, this occurs in the straight portion of the channel (x/d from 0 to 120) at $x/d \leqslant 108$. Constant Nu at x/d from 108 to 120 then indicate thermal boundary layers which are more fully developed with non-dimensional mean temperature profiles which approach streamwise invariance.

The developing thermal boundary layers ($x/d < 108$) are contained mostly within the low velocity portions of the momentum boundary layer where buoyancy induced motions have equivalent magnitudes. According to Maughan and Incropera [31], such buoyancy induced secondary flows augment Nu over pure forced convection values in channels between horizontal parallel plates. When inclined and non-horizontal, buoyancy forces in such channels can enhance Nusselt numbers compared to those expected for laminar forced convection alone, especially for large heat rates and low flow rates.

When channel thermal layers merge to become fully developed, the opposite trend is seen in the present study. At $x/d > 108$, Figs. 3–5 show that buoyancy induced motions reduce Nusselt numbers compared to pure forced convection values. At each x/d, Nu decreases continually as Gr increases. Velocities induced by natural convection with this situation are generally significantly less than streamwise advection velocities associated with the forced flow. Thus, the effect of the buoyant motions is to reduce the forced flow velocities and impede the flow especially near channel surfaces, much like mixed convection environments wherein buoyancy is aligned with the forced flow and directly impedes the forced flow. In addition, near wall gradients of mean temperature are probably altered and often diminished by the secondary flows induced by buoyancy. Results presented by Shai and Barnea [5] are consistent since they also predict mixed convection Nusselt numbers less than Nu_{FC} for opposed laminar mixed convection near vertical surfaces.

The developing thermal boundary layers from the present study ($x/d < 108$) also produce Nu in Figs. 4 and 5 which decrease with Gr at each x/d. The only difference is that $Gr = 0$ ($\beta\Delta t = 0$) values are sometimes slightly higher than ones expected for pure forced convection. As mentioned earlier, this is due to relatively thin thermal boundary layers at small x/d which are located entirely in low velocity portions of the velocity boundary layer where buoyancy induced velocities and motions dominate. The buoyancy induced motions in this situation may thus *locally* augment advection very near channel surfaces giving mixed convection Nu which may be locally higher than Nu_{FC} values.

Effects of curvature

Another interesting feature of Figs. 4 and 5 is evident if the forced convection Nusselt numbers ($Gr = 0$) from the concave and convex surfaces are compared. Of importance here is the unstable stratification of angular momentum which develops in the flow due to concave curvature of streamlines. Centrifugal instabilities and the subsequently developing secondary flows then result in concave surface Nusselt numbers at $x/d > 120$ which are consistently higher than convex values when compared at the same Re and channel location. These secondary flows first appear at low Re in the form of arrays of tiny Görtler-like vortices near the concave surface. These become larger in span and radial directions with streamwise development. Eventually, an array of counter-rotating Dean vortex pairs are present across the entire span of the channel [42–45]. The secondary flows and unsteadiness from the initial development of the Dean vortices is responsible for the Nusselt number increase with x/d on the concave surface, and concave Nu which are higher than convex Nu as x/d becomes just greater than 120 [42]. The twisting secondary instability [43, 44] is then responsible for the second Nusselt number increase with x/d on the concave surface (Fig. 4) which occurs as x/d increases from 180 to 204 [42]. Because these phenomena initially have little impact on flow behavior near the convex surface, similar Nusselt number increases at corresponding x/d are not apparent in Fig. 5.

Examination of Figs. 4 and 5 also reveals that these

phenomena due to curvature also affect mixed convection Nusselt numbers. This is especially evident from the concave surface results for individual Gr from 14.9×10^6 to 27.1×10^6 in Fig. 4, since each Nu distribution shows an increase with x/d, as x/d increases from 108 to 132, and as x/d increases from 180 to 204. Thus, secondary flows from two different mechanisms influence local Nusselt number magnitudes. (i) Buoyant motions near channel surfaces act *locally* to impede the local flow causing local Nu at each x/d to decrease with increasing Gr as the magnitude of buoyant forces increase relative to the forced flow. (ii) At each Gr, curvature induced secondary flows then simultaneously act to vary Nu distributions with streamwise development, particularly on the concave surface. Convex surface Nusselt numbers in Fig. 5 are consistent, since qualitative trends with x/d for each Gr from 15.1×10^6 to 27.5×10^6 are similar to the pure forced convection ($Gr = 0$) data trend.

MIXED CONVECTION WITH STRONG BUOYANCY

Nusselt number dependence on Grashof number

Results illustrating Nusselt number behavior with strong buoyancy are presented in Fig. 6. Here, measured Nu are plotted as a function of Gr, V_c^2 and $\beta\Delta t$ for concave and convex channel surfaces at $Re = 343$. As for the results in Fig. 3, data points are plotted *vs* $\beta\Delta t$ and V_c^2, and the Gr scale is approximate because of the variations of kinematic viscosity with temperature. Forced convection Nu in Fig. 6 are located on the left-hand side of the plot at $Gr = 0$ ($\beta\Delta t = 0$), and pure natural convection data [40] lie at the right-hand portion of the data distribution at Gr from 35×10^6 to 45×10^6 ($\beta\Delta t$ from 0.05 to 0.07). The data in Fig. 6 are given for $x/d = 108$ because this value corresponds to the downstream end of the straight portion of the channel where the thermal flow is at or near a fully developed condition. As mentioned earlier, simple analysis of this flow gives a pure forced convection Nu of 8.24, and thus, the magnitude of Nu is known at $Gr = 0$ in Fig. 6.

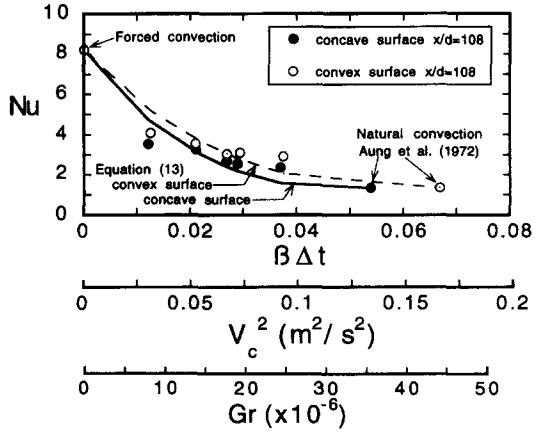

Fig. 6. Measured mixed-convection Nusselt numbers, deduced forced convection Nusselt numbers, and natural convection Nusselt numbers as dependent upon Gr, V_c^2, and $\beta\Delta t$ to illustrate mixed convection with strong buoyancy for $Re = 343$ and $x/d = 108$ (at downstream end of the straight portion of the channel).

Correlation of data for mixed convection with strong buoyancy

In contrast to the results in Fig. 3, Nu data in Fig. 6 are non-linear with V_c^2 and $\beta\Delta t$ because of strong buoyancy influences on the temperature field. The data are well correlated using an equation of the form

$$Nu = Nu'\alpha + Nu_{FC}(1-\alpha) + (Nu_{NC} - Nu')\alpha^{1.5} \tag{13}$$

where $Nu' = -14.0$ for $Re = 343$. Equation (13) is valid for mixed convection with *strong* buoyancy. The last term thus accounts for the non-linear portion of the dependence of Nu on α within this regime. As Re increases from 343 to 686, buoyancy effects become weaker relative to the forced flow. Nu' then first increases, becomes positive, and then approaches Nu_{NC}. The last term in equation (13) thus becomes less important as Re increases. When $Re \geqslant 686$, and mixed convection with *weak* buoyancy is present, Nu' equals Nu_{NC} and the last term in equation (13) is zero.

Effects of strong buoyancy and curvature

Mixed convection with strong buoyancy exists for $Re < 646$. This regime is characterized by $V_c/U > 0.35$ and magnitudes of buoyancy-induced secondary flows which are significant relative to the forced flow bulk velocity *across most of the channel cross-section.* Within this regime, there are two sub-regimes which result as Reynolds number decreases (at constant Grashof number) and the buoyancy induced secondary flows increase in intensity relative to forced flow motions.

The first sub-regime probably exists at Reynolds numbers from about 500 to 686. Here, both Dean vortex pairs and buoyancy-induced secondary motions have important influences on local flow behavior and local heat transfer. Interactions likely result in a quite complicated three-dimensional flow field.

The second sub-regime at Re lower than about 500 is different from the first because secondary motions induced by buoyancy are dominant, and centrifugally induced secondary motions, relatively speaking, are much less important. According to Ligrani and Niver [43], there is little evidence of curvature induced secondary flows at these conditions. The strong buoyancy effects then produce non-linearity, strong coupling with the momentum equation, and complicated convolutions of the temperature field, especially near walls. All of these are responsible for the behavior characterized by equation (13) and the results presented in Fig. 6, which are then representative of fully

developed thermal flow behavior regardless of the amount of curvature.

Important and complex secondary flows and temperature field convolutions induced by buoyancy are also present in other geometries with laminar forced flow. In straight horizontal tubes, Coutier and Greif [46, 47] observe strong three-dimensional, and large circumferential variations of fluid temperature and Nusselt number from buoyancy. The mixed convection flows are categorized at different flow conditions using Gr/Re^2, and change significantly as different thermal boundary conditions are imposed [47].

REGIMES OF BEHAVIOR

Nusselt number data for natural, mixed, and forced convection from the present study are plotted in Fig. 7 as a function of Gr/Re^2. Data are presented for channel Reynolds numbers of 343, 686, 1371 and 2057 to illustrate the effects of a wide range of this parameter. All pure natural convection data points are determined from Aung *et al.* [40].

Regardless of the Reynolds number, forced convection Nu data lie on the ordinate at $Gr/Re^2 = 0$ in Fig. 7, and pure natural convection values are located at the right-hand side of each collection of data. Mixed convection data of course are distributed in between the natural convection and forced convection data. As the Reynolds number increases, the mixed convection data are located at smaller values of Gr/Re^2, and spread over a smaller portion of the graph over a smaller range of Gr/Re^2.

The boundary between mixed convection data with strong buoyancy and mixed convection data with weak buoyancy is apparent from the data presented in Figs. 3–7. Data trends in these figures indicate that this boundary is approximately associated with a Reynolds number just less than 686. The boundary is expressed in more general form using

$$Gr/Re^2 = 50 \qquad (14)$$

which is equivalent to $V_c/U \approx 0.35$. At Gr/Re^2 higher than 50, buoyancy effects are strong, and equation (13) provides a good representation of mixed convection data where Nu data are non-linearly dependent either upon V_c^2 or $\beta\Delta t$. This non-linearity due to strong buoyancy thus decreases as Gr/Re^2 decreases (i.e. as the Reynolds number increases at constant Grashof number). At values of Gr/Re^2 which are then lower than 50, buoyancy effects are then relatively weak, mixed convection Nusselt number data are linearly dependent upon V_c^2 (or $\beta\Delta t$), and the data are well correlated using equations (11) and (12). As Gr/Re^2 decreases further, Nu data show smaller variations with V_c^2 and $\beta\Delta t$. Eventually, at very low Gr/Re^2 near 0, Nu data will show no dependence upon Gr, V_c^2, or $\beta\Delta t$.

The $Gr/Re^2 = 50$ boundary is indicated in Fig. 7 for

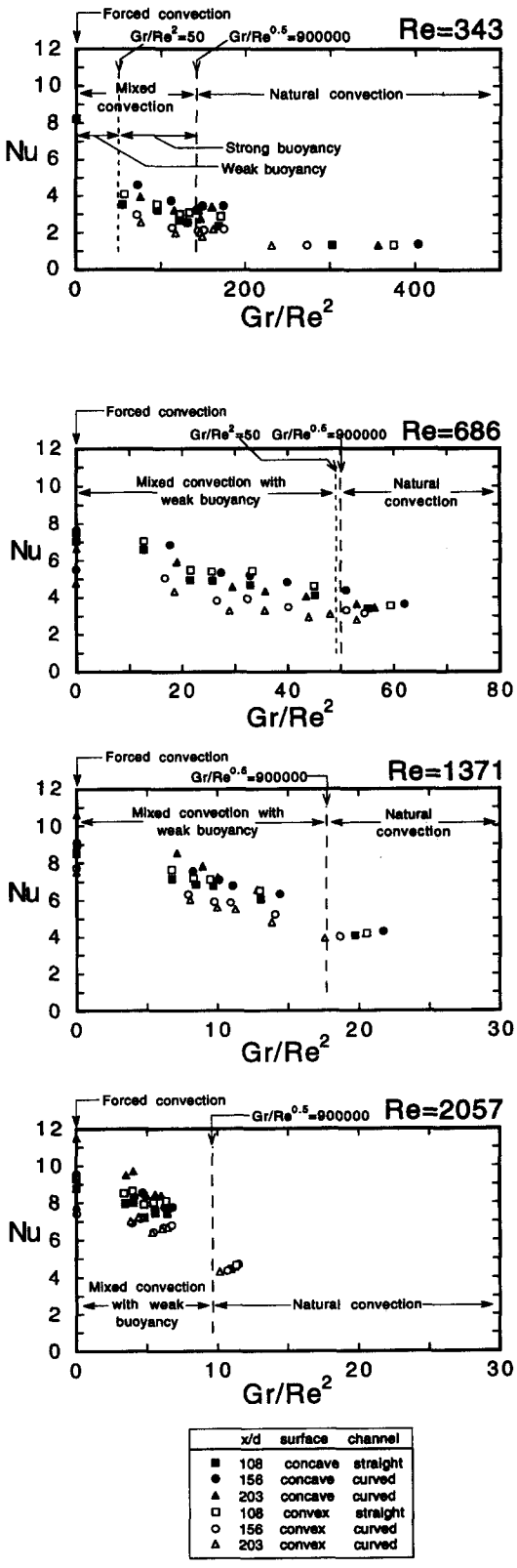

Fig. 7. Nusselt numbers as dependent upon Gr/Re^2 for Reynolds numbers of 343, 686, 1371 and 2057.

Re of 343 and 686. This boundary is not shown at higher Re where the present mixed convection data

do not show a clear distinction between weak buoyancy and strong buoyancy. Equation (14) coincides with a Peclet number of about 6, where Peclet number is given by

$$Pe = Pr(Ud^2/4vl).$$

According to Gebhart *et al.* [48], similar Pe values (from 4 to 6) separate pure natural convection from mixed convection between two vertical surfaces when buoyancy forces and bulk flows are *aligned*. Shai and Barnea [5] also observe distinctly different mixed convection regimes in *opposing* mixed convection over vertical plates with constant heat flux. They describe these as forced convection dominant and natural convection dominant, which are equivalent to mixed convection with weak buoyancy and mixed convection with strong buoyancy, respectively, in our terminology. Shai and Barnea employ a parameter analogous to V_c/U to separate the two regimes just like the present work. A parameter similar to the one given in equation (14) is also employed by Shai and Barnea [5] for *assisting* mixed convection over vertical flat plates with uniform heat flux. According to them, $Gr_x^{*2/5}/Re_x$ characterizes different convection regimes, where Gr_x^* is based on surface heat flux and vertical streamwise distance.

Figure 7 shows that pure natural convection Gr/Re^2 values range from 10 to 400, and that natural convection Nu data [40] at different Re do not collect into one range of Gr/Re^2 values. A better collapse is obtained using $Gr/Re^{0.5}$. According to Choi [37], $Gr/Re^{0.5}$ values for the present pure natural convection Nu data are 0.9×10^6–1.2×10^6 for $Re = 686$, 1371 and 2057. At $Re = 343$, $Gr/Re^{0.5}$ values for pure natural convection vary from 0.9×10^6 to 2.5×10^6. Thus, this parameter is not only the best one to characterize the pure natural convection data, but also the best one to characterize the boundary between the pure natural convection regime and the regime of mixed convection with strong buoyancy. The boundary between these regimes is then indicated on Fig. 7 for all Re, and is given in its most general form by:

$$Gr/Re^{0.5} = 900\,000. \quad (15)$$

Figure 7 then shows that magnitudes of $Gr/Re^{0.5}$ greater than 0.9×10^6 characterize pure natural convection. Values below indicate mixed convection with weak buoyancy at Re of 686, 1371 and 2057, and mixed convection with strong buoyancy at $Re = 343$.

A summary of the extents of all observed convection regimes from the present study is presented in Fig. 8 using *Gr vs Re* coordinates. Ranges of measured mixed convection data for $Re = 343$, 686, 1371 and 2057 are included for comparison. From this figure, the $Gr/Re^2 = 50$ regime boundary applies only for $Re < 687$. At Reynolds numbers less than 687, Grashof number increases from zero first produce pure forced convection, followed by mixed convection with weak buoyancy, mixed convection with strong buoyancy, and then pure natural convection. Alternatively, if Reynolds number increases from zero at constant Grashof number greater than 10×10^6, the flow order is pure natural convection, mixed convection with strong buoyancy, and mixed convection with weak buoyancy.

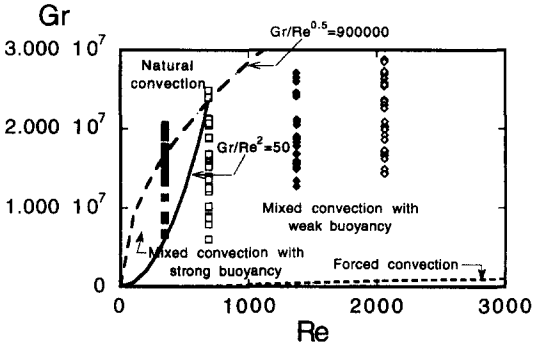

Fig. 8. Regimes of observed behavior.

SUMMARY AND CONCLUSIONS

New mixed convection experimental data are presented for a channel with curved and straight sections arranged so that buoyancy induced motions are orthogonal to the forced flow. The top and bottom surfaces of the channel are closed, aspect ratio is 40, and constant heat flux boundary conditions are imposed on the surfaces. Pure natural convection is present when $Gr/Re^{0.5} > 900\,000$, and pure forced convection is present for Gr/Re^2 values near zero. Between, two regimes of mixed convection are observed. Mixed convection with *strong* buoyancy is present when $Re < 687$, $Gr/Re^2 > 50$, and $Gr/Re^{0.5} < 900\,000$. For $Re < 687$, mixed convection with *weak* buoyancy is then observed for $Gr/Re^2 < 50$. For $Re > 687$, mixed convection with *weak* buoyancy is observed for $Gr/Re^{0.5} < 900\,000$. In both mixed convection regimes in both the curved or straight portions of the channel, orthogonal buoyancy is qualitatively similar to *aligned opposing* mixed convection because mixed convection Nusselt numbers are generally less than pure forced convection values.

When mixed convection with *weak* buoyancy is present, the orthogonal flow fields weaken the non-linearity and coupling within the field equations so that mixed convection Nu vary linearly with $\beta\Delta t$ or V_c^2 between pure forced convection and pure natural convection limits. Consequently, Nusselt numbers are well correlated by equation (11). With this equation, pure forced convection Nusselt numbers are easily and accurately determined from mixed convection Nusselt numbers measured at different Grashof numbers (or different V_c^2 and $\beta\Delta t$). Within this mixed convection regime, secondary flows from two different mechanisms influence local Nusselt number magnitudes. (i) Nu data at individual x/d show a systematic decrease

with increasing Gr and V_c regardless of thermal boundary layer development, and regardless of whether results are obtained in the straight or curved portions of the channel. This is the result of buoyancy induced velocities, which diminish near wall gradients of mean temperature, and *locally* reduce streamwise advection velocities and impede the flow, especially near channel surfaces. (ii) At each Gr, curvature induced secondary flows then simultaneously act to vary Nu distributions with steamwise development, particularly on the concave surface. The most important of these secondary flows result from initial vortex development [42, 43, 45] and vortex pair twisting [42–44].

When mixed convection with *strong* buoyancy is present, non-linearity, strong coupling in the field equations, and complicated convolutions of the temperature field, especially near walls are responsible for the non-linear dependence of Nusselt numbers on $\beta\Delta t$ and V_c^2 between pure forced convection and pure natural convection limits. At $Re < 500$, the secondary flow field is dominated by buoyancy induced motions since centrifugally induced secondary motions are practically non-existent. These buoyancy induced motions are believed to affect streamwise advection *globally* across most of the channel cross-section. Nusselt number data are then well correlated using equation (13).

Acknowledgements—The work presented was sponsored by the Propulsion Directorate, U.S. Army Aviation Research and Technology Activity-AVSCOM through NASA-Defense Purchase Request C-30030-P.

REFERENCES

1. L. N. Tao, On combined free and forced convection in channels, *ASME Trans. J. Heat Transfer* **82,** 233–238 (1960).
2. S. W. Churchill and R. Usagi, A general expression for the correlation of rates of transfer and other phenomena, *A.I.Ch.E. Jl* **18,** 1121–1128 (1972).
3. S. W. Churchill, A comprehensive correlating equation for laminar, assisting, forced and free convection, *A.I.Ch.E. Jl* **23,** 10–16 (1977).
4. R. Chilukuri and J. A. C. Humphrey, Numerical computation of buoyancy induced recirculation in curved square duct laminar flow, *Int. J. Heat Mass Transfer* **24,** 305–314 (1981).
5. I. Shai and Y. Barnea, Simple analysis of mixed convection with uniform heat flux, *Int. J. Heat Mass Transfer* **29,** 1139–1147 (1986).
6. W. Aung and G. Worku, Mixed convection in ducts with asymmetric wall heat fluxes, *ASME Trans. J. Heat Transfer* **109,** 947–951 (1987).
7. Y. Mori and Y. Uchida, Forced convection heat transfer between horizontal flat plates, *Int. J. Heat Mass Transfer* **9,** 803–817 (1966).
8. M. Akiyana, G. J. Hwang, and K. C. Cheng, Experiments on the onset of longitudinal vortices in laminar forced convection between horizontal plates, *ASME Trans. J. Heat Transfer* **93,** 335–341 (1971).
9. J.-W. Ou, K. C. Cheng and R.-C. Lin, Natural convection effects on the Graetz problem in horizontal rectangular channels with uniform wall temperature for large Pr, *Int. J. Heat Mass Transfer* **17,** 835–843 (1974).
10. S. Ostrach and Y. Kamotani, Heat transfer augmentation in laminar fully developed channel flow by means of heating from below, *ASME Trans. J. Heat Transfer* **97,** 220–225 (1975).
11. G. J. Hwang and C. L. Liu, An experimental study of convection instability in the thermal entrance region of a horizontal parallel-plant channel heated from below, *Can. J. Chem. Engng* **54,** 521–525 (1976).
12. Y. Kamotani and S. Ostrach, Effect of thermal instability on thermally developing laminar channel flow, *ASME Trans. J. Heat Transfer* **98,** 62–66 (1976).
13. Y. Kamotani, S. Ostrach and H. Miao, Convective heat transfer augmentation in thermal entrance regions by means of thermal instability, *ASME Trans. J. Heat Transfer* **101,** 222–226 (1979).
14. W. N. Gill and E. Del Casal, A theoretical investigation of natural convection effects in forced horizontal flows, *A.I.Ch.E. Jl* **8**(4), 513–518 (1962).
15. K. C. Cheng and C. J. Hwang, Numerical solution for combined free and forced laminar convection in horizontal rectangular channels, *ASME Trans. J. Heat Transfer* **91,** 59–66 (1969).
16. W. Nakayama, G. J. Hwang, and K. C. Cheng, Thermal stability in planar Poiseuille flow, *ASME Trans. J. Heat Transfer* **92,** 61–67 (1970).
17. K. C. Cheng, S. W. Hong and G. J. Hwang, Buoyancy effects on laminar heat transfer in the thermal entrance region of horizontal rectangular channels with uniform wall heat flux for large Prandtl number fluid, *Int. J. Heat Mass Transfer* **15,** 1819–1827 (1972).
18. G. J. Hwang and K. C. Cheng, Convection instability in the thermal entrance region of a horizontal parallel-plate channel heated from below. *ASME Trans. J. Heat Transfer* **95,** 72–78 (1973).
19. T. V. Nguyen, I. L. Maclaine-Cross and G. de Vahl Davis, Combined forced and free convection between parallel plates. In *Numerical Methods in Thermal Problems* (Edited by R. W. Lewis and K. Morgan), pp. 269–278. Pine Ridge Press, Pine Ridge (1979).
20. K. J. Kennedy and A. Zebib, Combined free and forced convection between horizontal parallel planes: some case studies, *Int. J. Heat Mass Transfer* **26,** 471–478 (1983).
21. M. M. M. Abou-Ellail and S. M. Morcos, Buoyancy effects in the entrance region of horizontal rectangular channels, *ASME Trans. J. Heat Transfer* **105,** 924–927 (1983).
22. D. G. Osborne and F. P. Incropera, Laminar, mixed convection heat transfer for flow between horizontal parallel plates with asymmetric heating, *Int. J. Heat Mass Transfer* **28,** 207–217 (1985).
23. F. P. Incropera, A. L. Knox and J. R. Maughan, Mixed-convection flow and heat transfer in the entry region of a horizontal rectangular duct, *ASME Trans. J. Heat Transfer* **109,** 434–439 (1987).
24. F. C. Chou and G. J. Hwang, Vorticity-velocity method for the Graetz problem and the effect of natural convection in a horizontal rectangular channel with uniform wall heat flux, *ASME Trans. J. Heat Transfer* **109,** 704–710 (1987).
25. F. C. Chou and G. J. Hwang, Buoyancy effects on laminar forced convection in the thermal entrance region of horizontal rectangular channels, *ASME Trans. J. Heat Transfer* **112,** 250–253 (1990).
26. C. Nonino and S. Del Giudice, Laminar mixed convection in the entrance region of horizontal rectangular ducts, *Int. J. Numer. Meth. Fluids* **13,** 33–48 (1991).
27. F. C. Chou and G. J. Hwang, Combined free and forced laminar convection in horizontal rectangular channels for high ReRa, *Can. Chem. Engng* **62,** 830–836 (1984).
28. F. P. Incropera and J. A. Schutt, Numerical simulation

of laminar mixed convection in the entrance region of horizontal rectangular ducts, *Numer. Heat Transfer* **8,** 707–729 (1985).
29. H. V. Mahaney, F. P. Incropera and S. Ramadhyani, Development of laminar mixed convection flow in a horizontal rectangular duct with uniform bottom heating, *Numer. Heat Transfer* **12,** 137–155 (1987).
30. H. V. Mahaney, F. P. Incropera and S. Ramadhyani, Effect of wall heat flux distribution on laminar mixed convection in the entrance region of a horizontal rectangular duct, *Numer. Heat Transfer* **13,** 427–450 (1988).
31. J. R. Maughan and F. P. Incropera, Regions of heat transfer enhancement for laminar mixed convection in a parallel plate channel, *Int. J. Heat Mass Transfer* **33,** 555–570 (1990).
32. M. Hasnaoui, E. Bilgen, P. Vasseur and L. Robillard, Mixed convective heat transfer in a horizontal channel heated periodically from below, *Numer. Heat Transfer* **20,** 297–315 (1991).
33. J. R. Maughan and F. P. Incropera, Secondary flow in horizontal channels heated from below, *Expts Fluids* **5,** 334–343 (1987).
34. J. R. Maughan and F. P. Incropera, Experiments on mixed convection heat transfer for airflow in a horizontal and inclined channel, *Int. J. Heat Mass Transfer* **30,** 1307–1318 (1987).
35. P. E. Skogerboe, Local and spatially averaged heat transfer distributions in a curved channel with 40 : 1 aspect ratio for Dean numbers from 50 to 200, M.S. Thesis, U.S. Naval Postgraduate School, Monterey, CA (1990).
36. A. R. Schallert, A. study of Nusselt number distributions in a curved channel, M.S. Thesis, U.S. Naval Postgraduate School, Monterey, CA (1992).
37. S. Choi, A study of surface heat transfer in a curved channel at low Dean numbers, M.S. Thesis, University of Utah, Salt Lake City, UT (1995).
38. P. M. Ligrani, B. A. Singer and L. R. Baun, Miniature five-hole pressure probe for measurement of mean velocity components in low speed flows, *J. Phys. E Scient. Instrum.* **22**(10), 868–876 (1989).
39. P. M. Ligrani, B. A. Singer and L. R. Baun, Spatial resolution and downwash velocity corrections for multiple-hole pressure probes in complex flows, *Expts Fluids* **7**(6), 424–426 (1989).
40. W. Aung, L. S. Fletcher and V. Sernas, Developing laminar free convection between vertical flat plates with asymmetric heating, *Int. J. Heat Mass Transfer* **15,** 2293–2308 (1972).
41. S. H. Park and C. L. Tien, An approximate analysis for convective heat transfer on thermally nonuniform surfaces, *ASME Trans. J. Heat Transfer* **112,** 952–958 (1990).
42. P. M. Ligrani, S. Choi, A. R. Schallert, and P. E. Skogerboe, Effects of Dean vortex pairs on surface heat transfer in curved channel flow, *Int. J. Heat Mass Transfer* **39,** 27–37 (1996).
43. P. M. Ligrani and R. D. Niver, Flow visualization of Dean vortices in a curved channel with 40 : 1 aspect ratio, *Phys. Fluids* **31,** 3605–3617 (1988).
44. P. M. Ligrani, W. H. Finlay, W. A. Fields, S. J. Fuqua and C. S. Subramanian, Features of wavy vortices in a curved channel from experimental and numerical studies, *Phys. Fluids A* **4,** 695–709 (1992).
45. P. M. Ligrani, J. E. Longest, M. R. Kendall and W. A. Fields, Splitting, merging and spanwise wavenumber selection of Dean vortex pairs, *Expts Fluids* **18,** 41–58 (1994).
46. J. P. Coutier and R. Greif, An investigation of laminar mixed convection inside a horizontal tube with isothermal wall conditions, *Int. J. Heat Mass Transfer* **28,** 1293–1305 (1985).
47. J. P. Coutier and R. Greif, Mixed laminar convection in a horizontal tube with natural convection around its boundaries, *Int. J. Heat Mass Transfer* **29,** 391–402 (1986).
48. B. Gebhart, Y. Jaluria, R. L. Mahajan and B. Sammakia, *Buoyancy-Induced Flows and Transport*. Springer, Washington (1988).